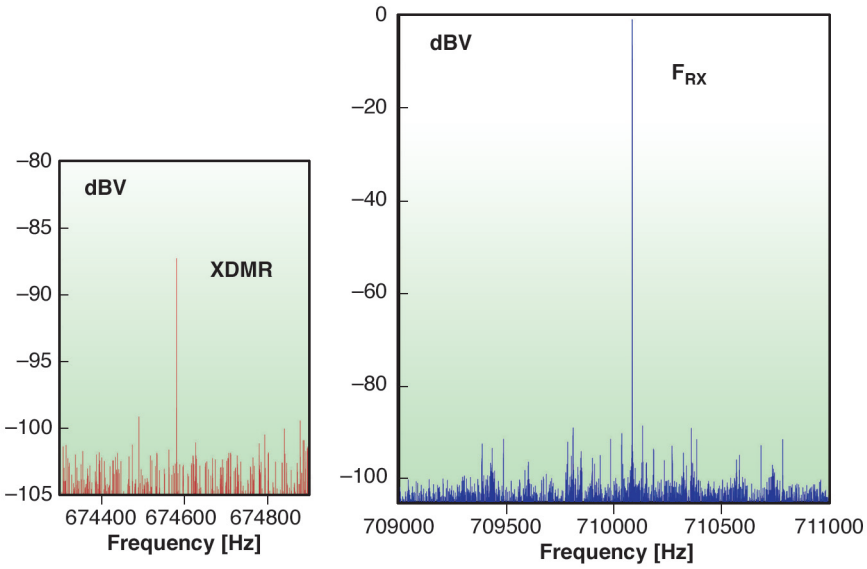


**Fig. 2:** XDMR signal as low-frequency side-band of $F_{RX}$.

storage ring was run in the 2*1/3 filling mode, the incident X-rays were modulated at the macrobunch repetition frequency $F_{RX}$ = 710.084 kHz. The XDMR signal displayed in **Figure 2** is one of the modulation side-bands expected at 710.084 ± 35.5042 kHz whereas the signal at $F_{RX}$ was used only for data renormalization. The magnitude of the XDMR signal is peaking *ca.* 20 dBV above the noise floor. The real and imaginary parts of the spectrum confirmed the expected inversion of the XDMR signal when the helicity of the incident X-ray beam was changed from Left to Right. After proper renormalization, the small differential cross-section: $\Delta\sigma_{XDMR} \approx 1.34 \cdot 10^{-5}$ would yield a critical precession angle of $\theta_{10} \approx 3.5°$ for the moments precessing at the Fe sites.

Since the effective operator accounting for XMCD at the Fe K-edge can be written [3]: $\partial/\partial E\ [<L_z>_{4p} + \varepsilon <L_z>_{3d}]$, the measured Fe K-edge XDMR signal thus produces clear evidence of the forced precession of orbital polarization components.

Let us emphasize that the precession angle $\theta_{10}$ deduced from XDMR for these orbital components is only one half of the critical precession angle $\theta_{crit}$ of the effective spin moment. Since the electron gyromagnetic ratios for orbital and spin moments are precisely in a 1:2 ratio, our XDMR result proves that, in YIG, there is *no* dynamical quenching of the magnetic orbital polarization components: spin-orbit coupling dominates orbit-lattice interactions in Kittel's picture of FMR.

## References

[1] J. Goulon, A. Rogalev, F. Wilhelm, N. Jaoen, C. Goulon-Ginet, G. Goujon, J. Ben Youssef and M.V. Indenbom, *JETP Letters*, **82**, (2005).

[2] A.G. Gurevich and G.A. Melkov: *Magnetization Oscillations and Waves*, CRC Press Boca Raton, Inc. (1996).

[3] H. Ebert, V. Popescu and D. Ahlers, *Phys. Rev. B* **60**, 7156 (1999).

## Principal Publication and Authors

J. Goulon (a), A. Rogalev (a), F. Wilhelm (a), N. Jaouen (a), C. Goulon-Ginet (a), G. Goujon (a),
J. Ben Youssef (b), M.V. Indenbom (b) *JETP Letters*, **82**, (2005)

*(a) ESRF*

*(b) Laboratoire de Magnètisme de Bretagne, CNRS FRE 2697, UFR Sciences et Techniques, Brest (France)*

# Plasma-assisted Magnetic Hardening of FePt Nanoparticles Investigated by X-ray Absorption

$Fe_xPt_{1-x}$ nanoparticles are currently the subject of intense research activity due to their interesting magnetic properties [1]. Chemically disordered $Fe_{50}Pt_{50}$ shows a high-temperature transformation to the ordered $L1_0$ phase which is associated with an enhancement of the orbital magnetic moment and a decrease of the mean distance between nearest-neighbour atoms by 2%. Therefore, on the one hand the x-ray absorption near edge structure (XANES) was analysed at the Pt $L_{3,2}$ edges to monitor structural changes, and on the other hand the x-ray magnetic circular dichroism (XMCD) was measured both at the Fe and Pt $L_{3,2}$ edges in order to investigate the orbital magnetism after thermal treatment.

The wet-chemically synthesised $Fe_{50}Pt_{50}$ particles with a mean diameter of 6 nm were self-assembled on a naturally oxidised Si substrate (total coverage: about 10%) and exposed to a soft hydrogen plasma (5 Pa for 30 min) that removes the Fe oxides and the organic ligands surrounding the particles in the as-prepared

state (**Figure 1**). Subsequently one of the samples was annealed at 600°C *in situ*. Scanning electron microscopy (SEM) images confirm the mean size, the centre-to-centre distance of 9 nm and a small agglomeration after annealing.

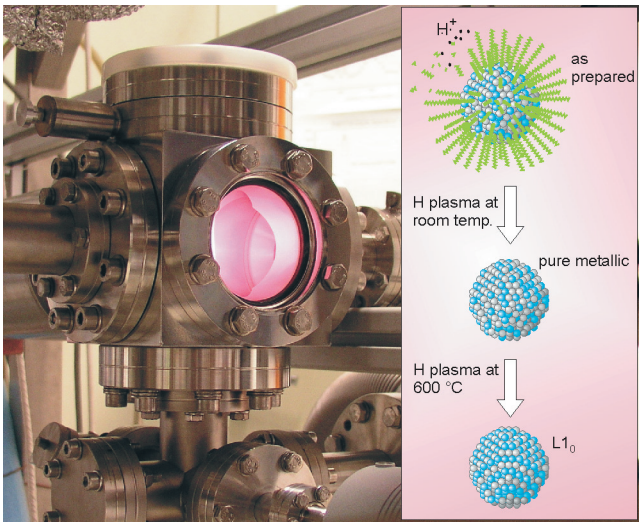


**Fig. 1:** Plasma chamber with ignited plasma. The inset shows schematically the removal of the organic ligands surrounding the wet-chemically synthesised $Fe_xPt_{1-x}$.

For measurements at the Pt $L_{3,2}$ edges, the UHV plasma chamber was attached to the experimental chamber at beamline **ID12** and the Fe oxides were removed prior to the experiments. In order to be able to record high quality XANES and XMCD spectra at the Pt $L_{3,2}$ edges on samples with such a low concentration of Pt, we have used a 35-channel silicon drift diode detector developed at the ID12 beamline in collaboration with Eurisys-Mesures (now Canberra Eurisys) [2]. During these experiments the counting rates in Pt $L_\alpha$ lines were *ca.* $2{\cdot}10^4$ cps per channel with a peaking time of 0.5 μs. Even though the X-ray beam was impinging on the sample with an angle of incidence of *ca.* 15°, the beam footprint was quite small: 300x30 μm². This is because we had to reduce the intensity of the monochromatic X-rays in order to avoid the saturation of the detector by the intense soft X-ray fluorescence signal from the substrates. The typical energy resolution of the emission spectra measured with one single SDD channel (data acquisition time: 60s; peaking time: 0.5 μs) was of the order of 132 eV for the unresolved Si $K_{\alpha\beta}$, 159 eV for the Fe $K_\alpha$ line and 202 eV for the Pt $L_{\alpha 1}$ line. Excellent performances of this detector allowed us to record not only the XANES spectra, but also the XMCD signals at

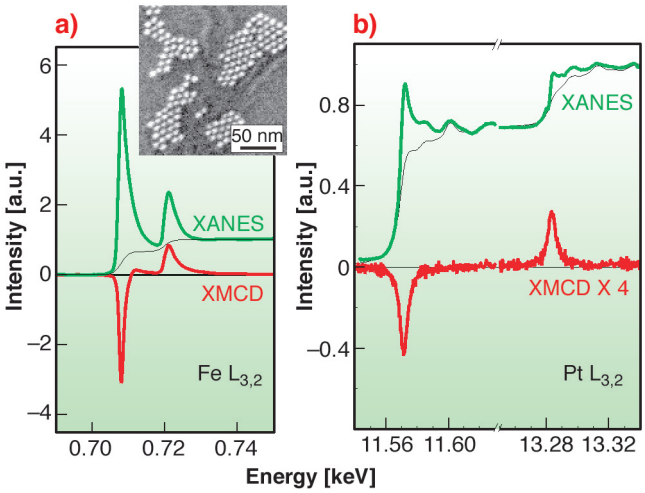


**Fig. 2:** XANES (green lines) and XMCD (red lines) of pure metallic $Fe_{50}Pt_{50}$ nanoparticles measured at the Fe and Pt $L_{3,2}$ edges. The dichroism spectra in (b) are scaled up by a factor of 4. The inset shows a SEM image of the sample.

the Pt $L_{3,2}$ edges in a weak magnetic field of ± 0.6 T (**Figure 2b**). The quality of the experimental data was high enough to derive the local spin and orbital magnetic moments of the Pt 5d states using the XMCD sum rules. The results of this analysis together with the analysis of the spectra recorded at BESSY, Germany, on the same samples at the Fe $L_{3,2}$ edges are given in **Table 1**.

The observed trends in $\mu_l$ / $\mu_S^{eff}$ indicate a non-cubic environment after annealing as expected for the $L1_0$ structure.

Additionally, we found that the period of the first EXAFS oscillations at the Pt $L_{3,2}$ edges decreased by (3±2)% after annealing indicating a reduction of the mean distance between the atoms as known for the disorder-order transformation in the corresponding bulk material.

In conclusion, we demonstrated a method to prepare pure metallic $Fe_{50}Pt_{50}$ nanoparticles from wet-chemically synthesised particles. Evidence for the formation of the $L1_0$ phase is provided both by structural changes found in the oscillations of the XANES and by the changes in the magnetic moments.

**Acknowledgement:**
This work was supported by the BMBF (05 ES3XBA/5), the DFG (SFB445), the EU (MRTN-CT-2004-005566, SyntOrbMag), and the ESRF.

| | Fe | | | Pt | | |
|---|---|---|---|---|---|---|
| | $\mu_S^{eff}$ [ $\mu_B$] | $\mu_l$ [$\mu_B$] | $\mu_l$ / $\mu_S^{eff}$ | $\mu_S^{eff}$ / $\mu_B$ | $\mu_l$ / $\mu_B$ | $\mu_l$ / $\mu_S^{eff}$ |
| disordered | 2.48(7) | 0.056(10) | 2.2% | 0.41(1) | 0.054(2) | 13% |
| annealed | 2.59(8) | 0.240(18) | 9.3% | 0.41(1) | 0.042(2) | 10% |

**Table 1:** Local spin and orbital magnetic moments for Fe and Pt.

**References**

[1] C. Antoniak, J. Lindner, and M. Farle, *Europhys. Lett.* **70**, 205 (2005).

[2] J. Goulon, A. Rogalev, G. Goujon et. al., *J. Synch. Rad*. **12**, 57 (2005).



**Principal Publication and Authors**

C. Antoniak (a), J. Lindner (a), M. Spasova (a), D. Sudfeld (a), M. Acet (a), M. Farle (a), K. Fauth (b,c), U. Wiedwald (d), H.-G. Boyen (d), F. Wilhelm (e), A. Rogalev (e), and Shouheng Sun (f), *submitted*.

*(a) Fachbereich Physik, Universität Duisburg-Essen (Germany)*

*(b) MPI für Metallforschung, Stuttgart (Germany)*

*(c) Experimentelle Physik IV, Universität Würzburg (Germany)*

*(d) Abteilung Festkörperphysik, Universität Ulm (Germany)*

*(e) ESRF*

*(f) Department of Chemistry, Brown University, Providence, RI (USA)*


# Evidence of Topological Defects in an Electronic Crystal

Electron confinement, for example along chains of atoms, give rise to original phenomena. These effects are observed in charge-density wave (CDW) materials. Upon cooling, these materials exhibit a modulation of the electron density along the chains and become insulating. Moreover, under a large enough electric field, a strong decrease of the resistivity is observed. This phenomena, still under debate, is generally interpreted as due to a collective "sliding" of the CDW as a whole [1].

This CDW can be considered as an electronic crystal, ordered in the three directions of space. In particular, its wave number along the chain is equal to twice the momentum of the fastest electrons of the system: $2k_F$. As any crystal, this electronic system is elastic and can exhibit dislocations. Predicted theoretically for 25 years [2], such topological defects are thought to play a essential role in the behaviour of the CDW under electric field, in a similar way dislocations in metals explain their plasticity.

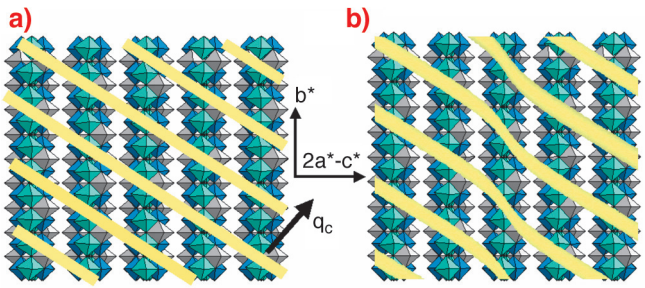


**Fig. 1:** Schematic representation of the Blue bronze CDW in the ( 2a*-c* ; b* ) plane in a) a defect-free crystal and b) a crystal with a screw-like dislocation line running along b* in the middle of the figure. Only Mo octahedra are represented. Yellow lines represent the constant phase wave front of the CDW. Note that this dislocation does not introduce any dilatation or compression of the CDW along b*.

The direct observation of CDW dislocations has never been achieved yet. Our recent experiment on the ID20 beamline has shown that coherent X-ray diffraction measurements are very sensitive to such topological defects. In the model system called "blue bronze" (a molybdenium oxide of formula $K_{0.3}MoO_3$), the structure of a CDW dislocation imbedded in the bulk has been studied. The interference fringes of the **Figure 2b** are interpreted as due to the presence of a screw dislocation running along the chain axis. Since the one-dimensional CDW wave vector $q_c$ is not parallel to the chains axis, this topological defect corresponds to a mixed dislocation (between screw and edge), running along the chains direction (see in **Figure 1b**). Remarkably, this dislocation introduce no energy expensive compression or dilatation of the CDW along the chains, but involves only shears: due to the charged character of the CDW, this is expected to cost less energy than an edge dislocation.

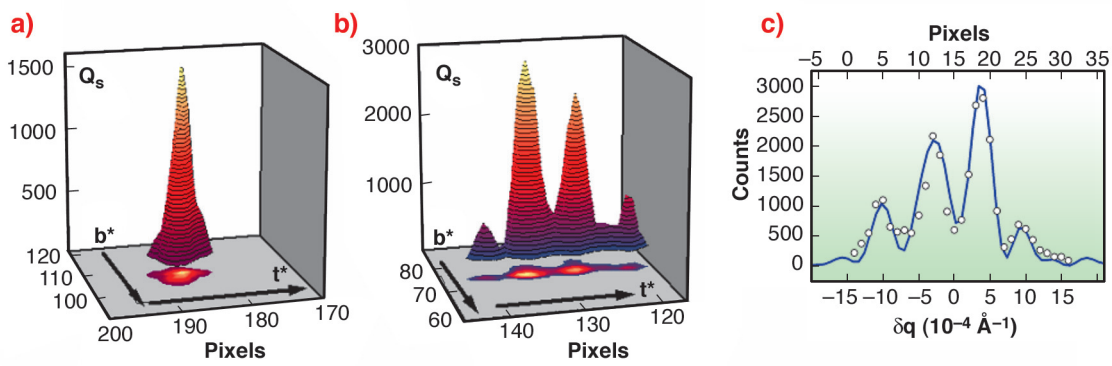


**Fig. 2:** 2D diffraction patterns of the $Q_s = (5,-1,-3)+q_c$ satellite reflection corresponding to a) Figure 1a and b) Figure 1b, at T = 75 K. c) Fit of the t*-scan of b) using the Fourier transform of the screw like dislocation shown in Figure 1b.